Electron impact excitation cross section studies of methane and acetylene

K. D. Pang, J. M. Ajello, and B. Franklin
Jet Propulsion Laboratory, California Institute of Technology, Pasadena, California 91109

D. E. Shemansky
Lunar and Planetary Laboratory, University of Arizona, Tucson, Arizona 85713

(Received 13 August 1986; accepted 21 November 1986)

We have measured the electron impact emission cross sections for CH_4 and C_2H_2 at 200 eV in a crossed beam laboratory system. Included in the study are all vacuum ultraviolet (VUV) emission features from 40 to 200 nm. The features are entirely from the atomic dissociation fragments (C I, C II, and H). The Lyman series of H is observed to truncate near principal quantum number $n = 10$ due to the long lifetime and to the high kinetic energy of the excited H fragments. The threshold region of the excitation functions has been measured at an energy resolution of 0.2–1.0 eV for the Lyman-α and Lyman-β transitions of H and C I (165.7, 193.1 nm) multiplets; and several distinct appearance potentials (AP) have been detected. For example, appearance potentials of Lyman-α from dissociation of CH_4 and C_2H_2 are noted at several energies, including the first observations of a Lyman-α AP from C_2H_2 at 16.3 eV.

I. INTRODUCTION

Although the electron impact excitation cross section of methane has been extensively studied in the laboratory other low-mass hydrocarbons have received little attention. It is instructive to do a comparative study of the electron impact excitation of methane with another simple organic molecule—acetylene. Even though methane CH_4 and acetylene C_2H_2 are the simplest of the classes of straight-chain hydrocarbons known as alkanes and alkynes, respectively, the electronic bonds in these molecules differ significantly. There are four single bonds in methane, i.e.,

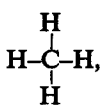

(1)

while acetylene contains a carbon–carbon π bond:

$$H\text{–}C\equiv C\text{–}H\,. \qquad (2)$$

Therefore, a comparison of the electron impact fluorescence spectra, rich in emission lines of dissociative excitation products, may reveal the physical processes that occur when energetic electrons collide with simple organic molecules.

The study of these two gases also has useful applications in aeronomy and astrophysics. Both gases have been found in the atmospheres of Jupiter, Saturn, Uranus, and Titan.[1,2] Methane has been identified in the atmosphere of Neptune; and acetylene is expected there also.[3] Lyman-α emissions have been detected from all five bodies, produced by a variety of excitation processes.[3,4] The Voyager 2 spacecraft encountered Uranus in early 1986 and discovered that the Lyman-α emissions of that planet are due to both auroral processes and to an "electroglow,"[2] both phenomena arising predominantly from electron impact excitation of H and H_2. A detailed study of UV emissions from H_2 [5] and revision of the benchmark cross section[6] for Lyman-α from dissociative excitation of H_2 have been obtained recently from the same experimental system described here. Laboratory studies of CH_4 and C_2H_2 by electron impact are applicable to the interpretation of Voyager UV spectrometer data and may contribute to understanding the composition and processes occurring in the upper atmosphere of the outer planets. The same C I multiplets observed in the laboratory may have been observed on Uranus,[2] although the excitation mechanism is likely to be different.

A comprehensive study of these gases calls for absolute cross section measurements, with particular emphasis on: (1) the appearance potentials (AP) for excited fragments; and (2) theoretical modeling of emission spectra and excitation functions. In addition a third subject of importance would be to perform kinetic energy studies of the excited fragments by linewidth or time of flight measurements. Of these, only the first two subjects will be reported in detail here. Our theoretical spectral modeling is limited to comparison of the Lyman-α series Rydberg system intensities of $e + H$, with the observed spectra of $e + CH_4$ and $e + C_2H_2$. The observations of VUV emission spectra at 0.5 nm resolution were made from 40 to 200 nm at 200 eV. Bethe–Born approximation analyses will be made on the high-energy region of the excitation functions to determine whether the production process of excited fragments proceeds via allowed electric dipole or forbidden transitions. A comparison of the laboratory AP with theoretical dissociation limits (DL) allows a determination of the candidate dissociation processes, along with the released reaction energy. Linewidth measurements are being made with our high-resolution ($0.01 < \Delta\lambda < 0.05$ nm) system. However, much needed information on the energetics of the processes contributing to dissociation can be inferred from: (1) the study of high Rydberg fragments in time of flight studies by Schiavone *et al.*[7] and Finn *et al.*,[8] and (2) AP measurements of the Balmer series and C I (193.1 nm) multiplet by Donahue *et al.*[9] The instrumentation and procedures used to obtain the present spectral data at 0.5 nm resolution are described in the next section.

II. EXPERIMENTAL

The experimental apparatus and VUV calibration techniques have been described in detail in earlier publica-

 0021-9606/87/052750-15$02.10

tions.[5,10–12] In brief, the instrument consists of an electron impact emission chamber in tandem with two UV spectrometers. A magnetically collimated beam of electrons is crossed with a beam of gas formed by a capillary array at a background pressure that can be varied from 1×10^{-7} to 3×10^{-4} Torr. The instrument is entirely automated for repetitive scans and interfaced with a computer. The electron gun is mounted on a rotatable table to allow a measurement of the angular distribution of the radiation field in order to correct the measured cross section for polarization effects. However the measurements reported here were made at a 90° angle between electron beam axis and optic axis, since no polarization effects are expected in the case of molecular dissociative excitation where many intermediate states contribute to the dissociation.[13]

The energy scale is calibrated by measuring the AP 21.2 eV, of the 58.4 nm He line. AP's determined for methane and acetylene are reproducible to about $\pm$ 0.5 eV.

The absolute cross section of CH_4 (121.6 nm) or C_2H_2 (121.6 nm) used to normalize the entire 200 eV VUV spectrum is determined by the relative flow technique developed at this laboratory.[14] In this method the Lyman-α fluorescence signal at 200 eV electron impact energy from H_2, the standard gas, is compared to the fluorescence signals from CH_4 (121.6 nm) or C_2H_2 (121.6 nm) emission produced by electron impact at 200 eV on CH_4 or C_2H_2, the unknown gas. The comparisons were made over a range of background gas pressures from 3×10^{-7} to 1×10^{-5} Torr to establish linearity of signal with pressure. For the comparison of the signal strengths in the linear region, a value of 5.15×10^{-18} cm^2 was used for the Lyman-α cross section from H_2 at 200 eV.[15] By this method we find the cross section of the CH_4 (C_2H_2) feature to be 4.37×10^{-18} cm^2 (3.22×10^{-18} cm) at 200 eV. The cross sections at other wavelengths are given in a separate publication.[16] In the relative flow method, where H_2 is used as the standard gas, care must be taken to properly subtract the underlying molecular Lyman and Werner bands from the H I 121.6 nm signal. We described this procedure based on our H_2 models[5] in another publication.[6] We judge there is an 8% uncertainty in our corrected Lyman-α cross section in Ref. 15 together with a 15% uncertainty in relative calibration. The signal statistics and repeatability of the measurements provide relative cross sections to 5% accuracy. The resultant root sum square uncertainty is 22% for the absolute cross sections given in Ref. 16. We will first discuss the extreme ultraviolet (EUV) and far ultraviolet (FUV) emission spectra of the two gases.

III. SPECTRAL DATA AND MODEL

We show in Figs. 1 and 2 the EUV (40–140 nm) and FUV (110–210 nm) spectra for the process $CH_4 + e$ (200 eV), and in Figs. 3 and 4 the EUV and FUV spectra for the process $C_2H_2 + e$ (200 eV). Each feature identified in the spectra is assigned a number that also appears in the first column of the tables in Ref. 16. Features in Figs. 1 and 3 are further identified by Rydberg series or spectroscopic notation. Note that the EUV spectra (Figs. 1 and 3) are calibrated only to 130 nm. The complete set of all H I, C I, and C II multiplets contributing to each identified feature is listed in

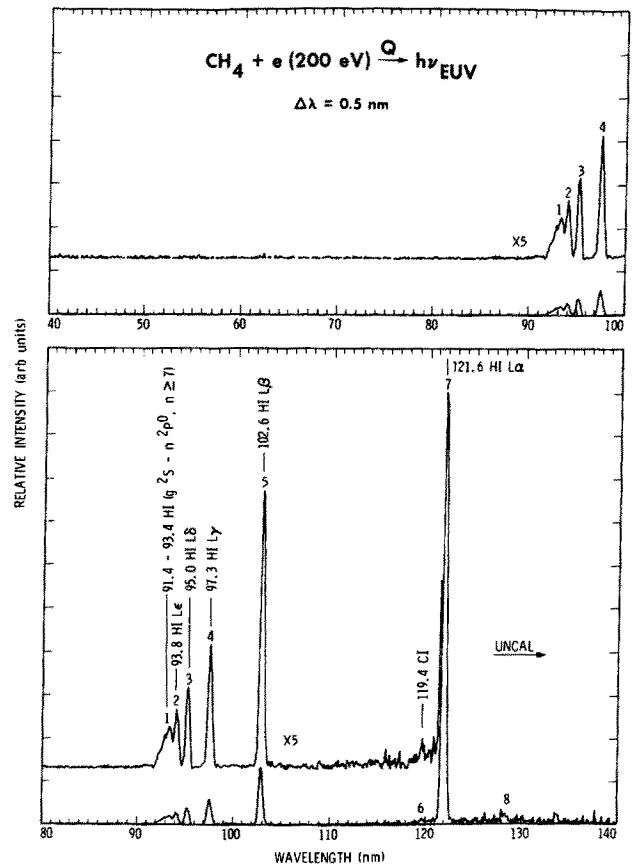

FIG. 1. Calibrated EUV spectrum of CH_4 at 200 eV electron impact energy at 0.5 nm resolution from 40 to 130 nm. The spectrum was obtained in the crossed beam mode at 4×10^{-6} Torr background pressure. Many of the features are identified by Rydberg series. The feature numbers are listed in Ref. 16 with identifications and cross sections.

the tables in Ref. 16. These identifications are taken from Kelly and Palumbo.[16] We have determined the cross section for each spectral feature by comparing its area relative to the area of Lyman-α whose cross section has been determined previously.[15] Total cross sections are given at the end of each table.[16–18]

At the resolution of 0.5 nm a total of 13 features were observed for methane. Features 1–5 and 7 are Lyman series emissions from H I that are to be discussed in greater detail, when compared with theoretical model predictions later. The rest of the features are emissions from excited carbon atoms and ions. Features 8 and 10–12 are C I lines, readily identifiable at 127.8, 146.3, 156.1, and 165.7 nm, respectively. Feature 13, the 193. 1 C I line, probably contains a small contribution from two C II transitions at nearly the same wavelength. Although excited with much less intensity, feature 6, a C I line at 119.4 nm can still be positively identified. Even at 0.5 nm resolution the C I line at 133.0 nm can be readily resolved from the C II line at 133.5 (feature 9).

The spectra for acetylene are richer than those for methane. In addition to the H I Lyman series emissions (features 5–9 and 13), the C I lines (features 12, 15, 19, 21, 22, and 24), and C II line (feature 17) also found for methane, additional C I lines (features 11, 14, 16, 18, 20, and 23) are identified at 115.8, 126.0, 131.3, 135.9, 148.2, and 175.2 nm, respectively. The C II transition at 90.6 nm has a small cross

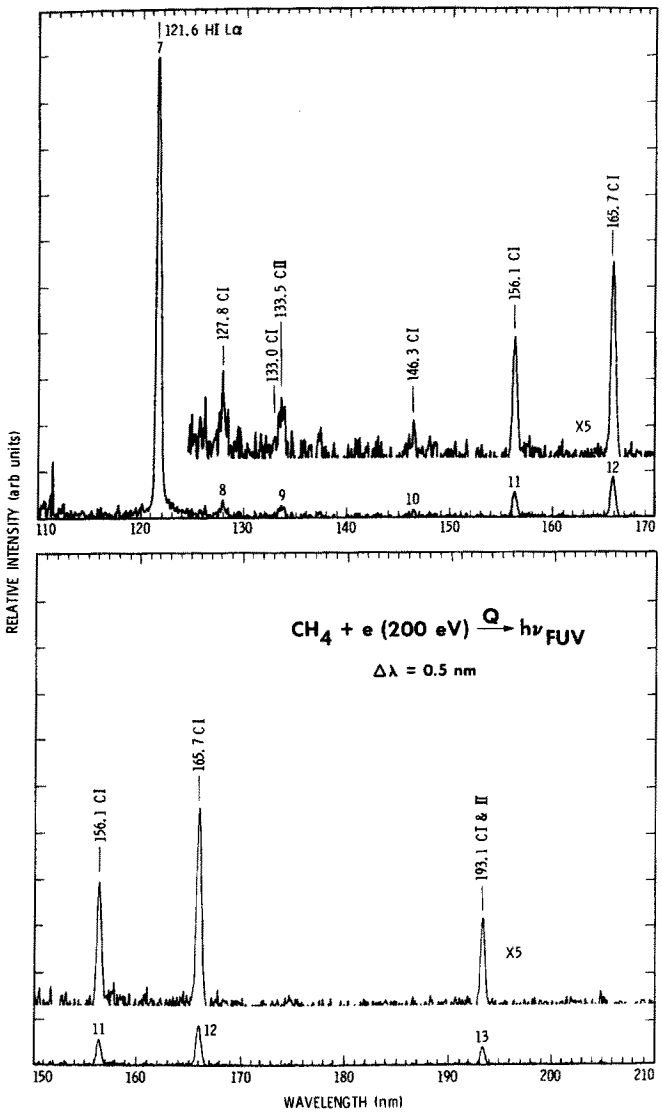

FIG. 2. Calibrated FUV spectrum of CH_4 at 200 eV electron impact energy at 0.5 nm resolution from 110 to 210 nm. The spectrum was obtained in the crossed beam mode at 4×10^{-6} Torr background pressure. The feature numbers are listed in Ref. 16 with identifications and cross sections.

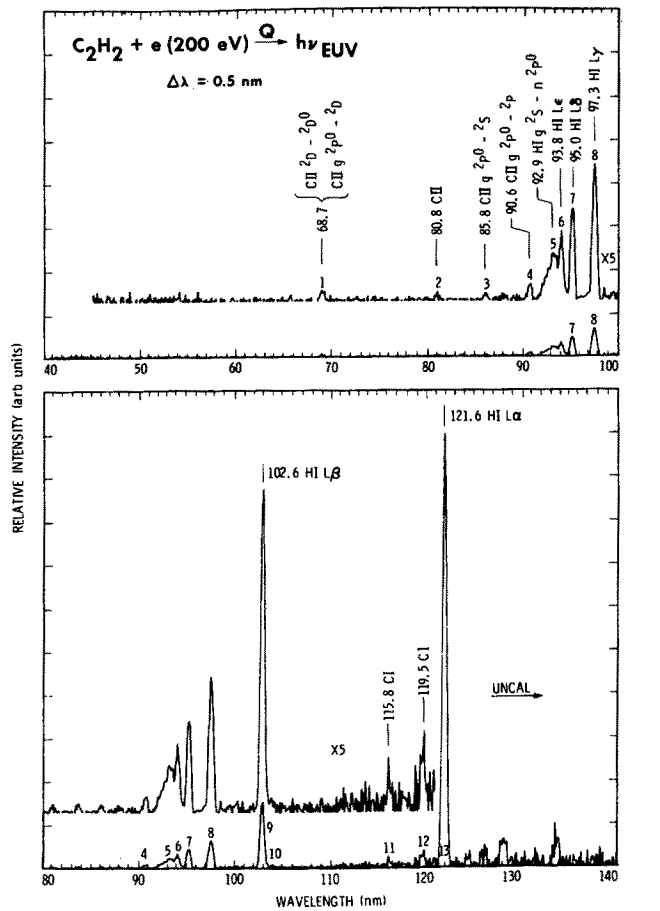

FIG. 3. Calibrated EUV spectrum of C_2H_2 at 200 eV electron impact energy at 0.5 nm resolution from 40 to 130 nm. The spectrum was obtained in the crossed beam mode at 4×10^{-6} Torr background pressure. Many of the features are identified by Rydberg series. The feature numbers are listed in Ref. 16 with identifications and cross sections.

section ($\sim10^{-21}$ cm^2)[19] for methane and is not seen in Fig. 1. However, this line (feature 4) can be easily identified in the spectrum of acetylene (Fig. 3, upper panel), as are even weaker C II emissions (features 1, 2, and 3) at 68.7, 80.8, and 85.8 nm, respectively. The weak C II feature at 192.8 nm is not resolved from the C I 193.1 nm line using the present instrumentation.

All identifiable EUV and FUV features can be attributed to emissions from excited hydrogen and carbon atoms and ions, that are fragments from the electron impact dissociation of CH_4 or C_2H_2. The original molecular structure appears to play only a minor role in the formation of the emission spectrum. Winters[20] found that CH_4 dissociates into neutral or ionic fragments with equal probability when impacted by electrons with energy between 50 to 500 eV. However, emissions from the high mass excited fragments, C_2, CH, and CH^+ occur in the near UV and visible, and were not studied with our present instrumentation. In addition the Balmer series emissions from H I[19–21] were not studied. The observed Lyman series is similar to that expected from electron impact excitation of H. We can learn more about the excitation–emission process by comparing the observed H I Lyman series from CH_4 and C_2H_2 in Figs. 1 and 3, respectively, with theoretically computed intensities from e + H, and such a comparison is presented in the rest of this section. As a first step we show in Figs. 5 and 6 the Lyman series emissions from CH_4 (dotted lines) and C_2H_2 (dash lines) compared with those predicted by an atomic hydrogen model (continuous line). Details of the model have been given by Shemansky and Ajello.[22] The ratios of the observational intensities (normalized to Ly-α) are similar for the two gases, but are different than theory. The Lyman system intensities from the experiment on C_2H_2 and CH_4 decreases with increasing quantum number, $2<n<6$, much more slowly than the Lyman system theory of e + H intensities. However, for quantum number $n>6$, the intensities from the e + H Lyman series decreases more slowly than from the e + CH_4 or C_2H_2 Lyman series. The experimental Lyman series is, in fact, truncated at about $n=10$. A comparison between the experimental observations of the Lyman series between 90 and 95 nm with the theoretical e + H model, shows that only ten Lyman series terms are sufficient for both CH_4 and C_2H_2 to match the experimental data below 94

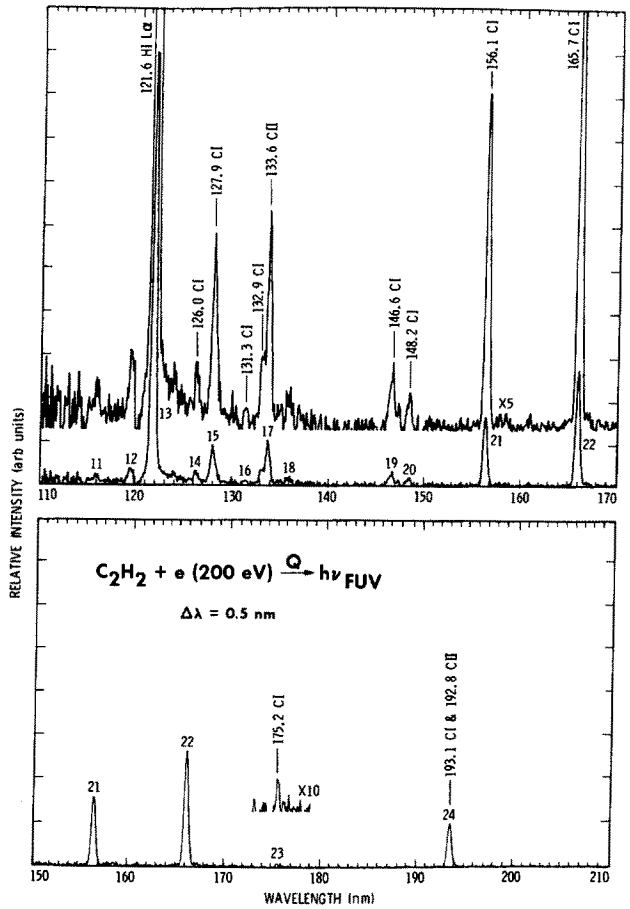

FIG. 4. Calibrated FUV spectrum of C_2H_2 at 200 eV electron impact energy at 0.5 nm resolution from 110 to 210 nm. The spectrum was obtained in the crossed beam mode at 4×10^{-6} Torr background pressure. The feature numbers are listed in Ref. 16 with identifications and cross sections.

nm. The three curves are shown in Fig. 6, normalized at 93 nm.

The most likely reason for the truncation of the H Rydberg series at $n = 10$ appears to be drift of excited atoms out of the field of view of the spectrometer. Radiative lifetimes of H Rydberg species increase in proportion to n^3. For $n = 10$, the lifetime $\tau = 0.79\times10^{-5}$ s.[23] Assuming a drift length of 25 cm, the required energy for loss of the atomic fragment is 5.2 eV. The lifetime of the H ($n\geqslant10$) atoms may also be limited by ionization caused by motional electric fields or electron impact; the energy threshold for ionization is very low.

The hydrogen atoms may thus have on the average a large amount of kinetic energy compared to thermal energy resulting in emission with a broadened linewidth.[24,25] Our AP studies, next section, indeed indicate that excited H-atom fragments are formed with several eV of translational kinetic energy.

From another aspect the cross sections we list in Ref. 16 for the Lyman series members with $10>n>7$ represent a lower limit, since some of these atoms diffuse out of the field of view in the direction transverse to the optic axes. We have previously solved this problem for the $N_2(a\,^1\Pi_g)$ metastable state.[12] The characteristic distance, y, perpendicular to the optic axis is 1 cm. Any motion of 1 cm or more, prior to radiating, will cause a loss of detected signal. Excited atoms of lifetime $\tau(n)$ traveling with a distribution of kinetic energies near 5.2 eV must radiate before moving 1 cm. This condition is satisfied if the lifetime is less than 10 times the transit time, t, that is if

$$t=\frac{y}{V}>\frac{\tau(n)}{10}, \tag{3}$$

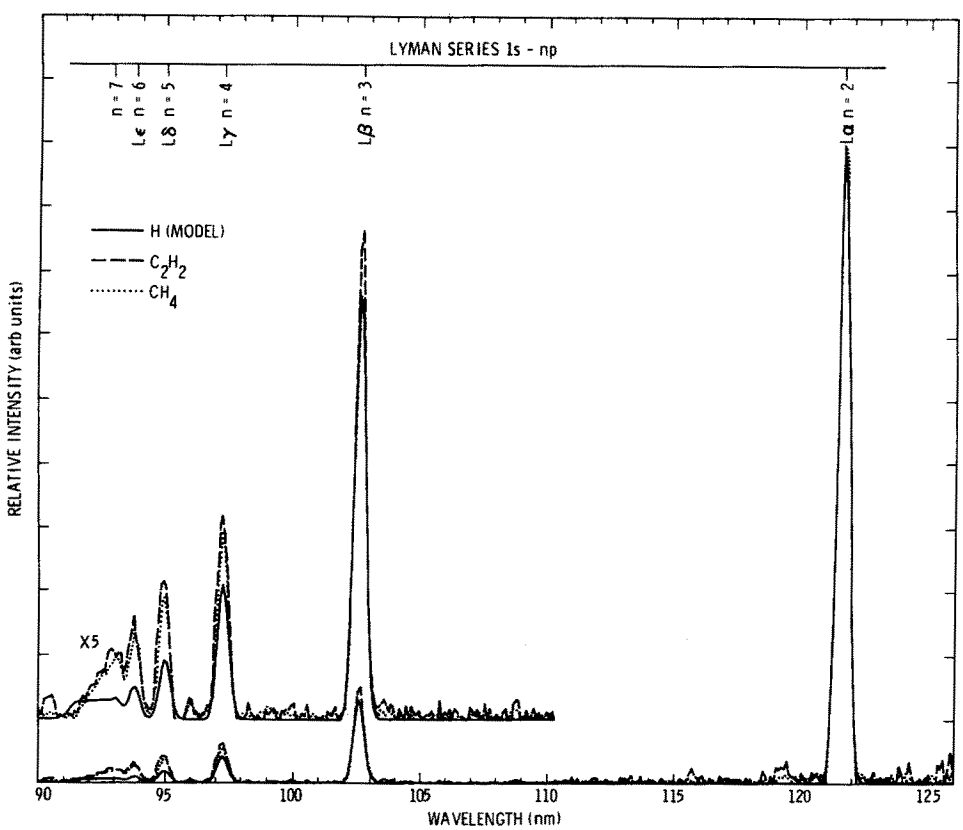

FIG. 5. Comparison of Lyman series from C_2H_2 and CH_4 data with an atomic H model. The data are from Figs. 1 and 3 at 200 eV electron impact energy. The atomic H model includes cascading to the Lyman series. The data are normalized at Lyman-α.

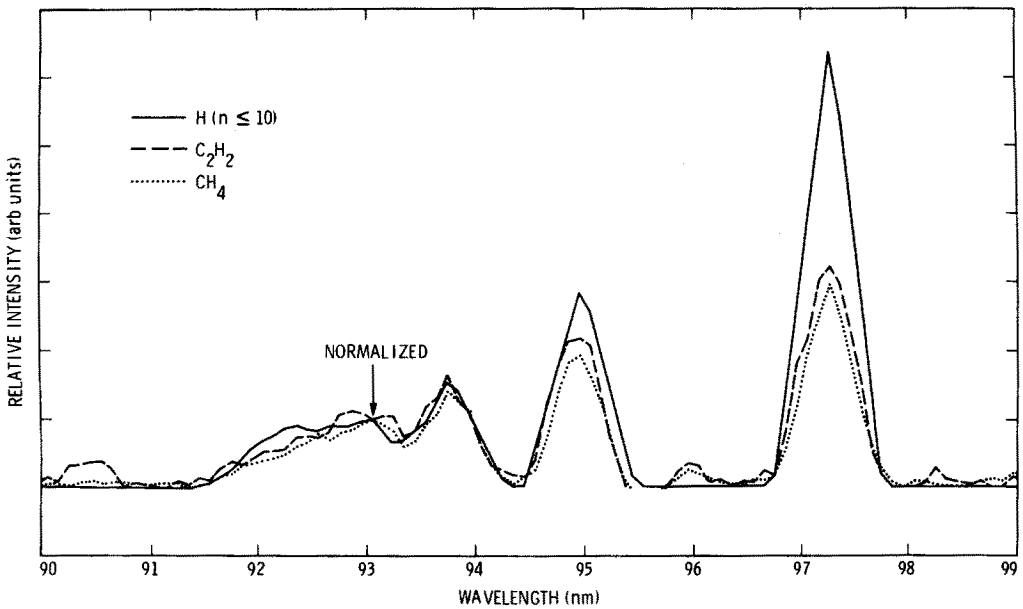

FIG. 6. Comparison of Lyman series from C_2H_2 and CH_4 data with an atomic H model that includes $n<10$. The data are from Figs. 1 and 3 at 200 eV impact energy. The data are normalized at 93.0 nm.

where V is the velocity of the excited atoms.

This calculation shows that Lyman-α to Lyman-ϵ features are unattenuated, the Lyman series $7 < n < 10$ are increasingly attenuated and $n > 10$ is absent. According to our models of H, cascading contribution from the *ns* and *nd* levels to the Lyman-α through Lyman-ϵ features contributes less than 5% of the intensity. The only features affected by the diffusion out of the field of view are feature numbers 1 of CH_4 in Fig. 1 and 5 of C_2H_2 in Fig. 3. Our cross section values for these features are lower limits. We now return to discussing the absolute cross sections of methane and acetylene.

IV. ABSOLUTE CROSS SECTIONS

The absolute cross sections as a function of energy from 0–400 eV were measured for the strongest features in the VUV spectra of CH_4 and C_2H_2 shown in Figs. 1–4. The relative cross section as a function of energy is plotted for all cases except for Lyman-α emission from CH_4, where the absolute cross section is plotted. For CH_4 we show Lyman-α in Fig. 7, Lyman-β, C I (165.7 nm), C I (193.1 nm) in Fig. 8. For C_2H_2 we show Lyman-α, Lyman-β, and C I (165.7 nm) in Fig. 9. In addition, we list absolute cross sections as a function of energy in Table I. Normalization of relative excitation functions to an absolute scale is based on our absolute value at 200 eV.[16]

Past laboratory experiments conducted on methane have produced widely different results. The H Lyman-α line is the strongest transition in the VUV spectra of both CH_4 and C_2H_2. Values for the absolute cross section for H Lyman-α emission by electron impact on methane at 100 eV differ by over an order of magnitude.[19,26–30] C_2H_2 has not been previously studied. Even the relative shape of the Lyman-α excitation function was not well-known[19,26–30] (see Fig. 7). Some of the earlier measurements suffered from limitations such as the use of a static gas target.[17,28,29] Molecular beams were later used, and the relative flow method eliminated some of the early experimental uncertainties.[30] However, major errors still remained. The worst of these being the normalization of the methane cross section to the "benchmark" cross section for Lyman-α from excitation of H_2, which has been found to be 60% too high due to failure to properly separate the Lyman-α emission from the molecular Rydberg emissions.[6] Other sources of the discrepancy may be caused by normalization to other absolute cross sections, e.g., O I (130.4 nm)[28] which also depends on dissociative excitation of H Lyman-α as a reference.

Of the six other absolute cross section measurements shown in the lower panel of Fig. 7, the values of Orient and Srivastava[30] are closest to ours. This is not surprising as their measurements were also obtained at the same scattering angle, 90°, and with the same relative flow method as the present experiment. Perhaps more importantly we have renormalized their methane cross sections to the new cross section for H Lyman-α at 100 eV.[15] The difference in the shape of the curves remains to be explained.

Similarly large discrepancies exist for the absolute methane cross section at other wavelengths. McLaughlin and Zipf[31] found that the cross section for the dissociative excitation of H Lyman-β by electron impact is 17.1×10^{-19} cm^2 at 100 eV. This value is nearly six times greater than that obtained by Vroom and de Heer.[26] However, it is based on an N I (120.0 nm) calibration cross section of 6.7×10^{-18} cm^2 at 100 eV. Table I shows that our H Lyman-β cross section at 100 eV is 8.6×10^{-19} cm^2, in excellent agreement with the value 10.2×10^{-19} cm^2 from McLaughlin and Zipf[31] when we apply the correction to the N I (120.0 nm) cross section given by Ajello and Shemansky[12] and the additional 11% reduction given in Ref. 15. Table I shows that the H Lyman-β cross section is nearly eight times less than that for H Lyman-α. It is thus not surprising that the excitation function for Lyman-β (Fig. 8) shows much more scatter than that for Ly-α (Fig. 7), despite a much longer integration time and the three-point running average of the data in Fig.

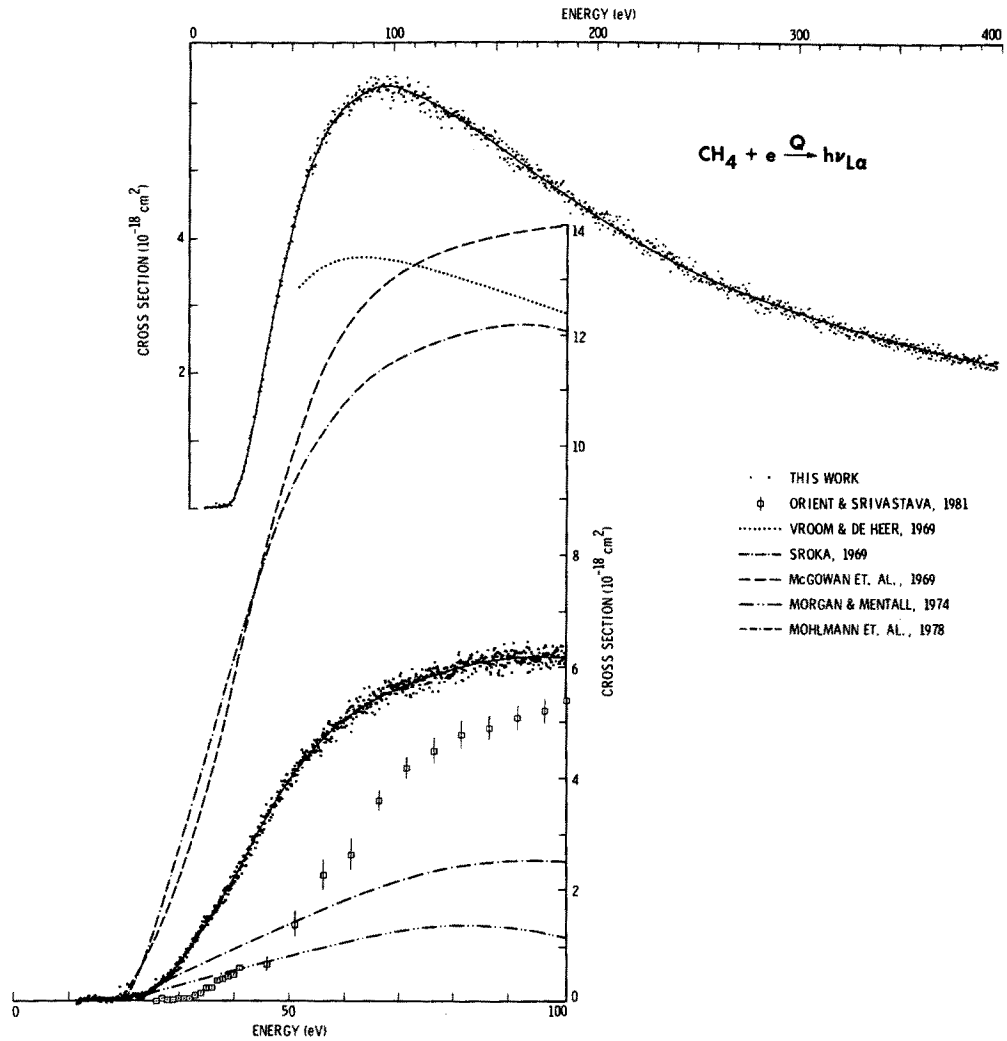

FIG. 7. Absolute emission cross section of the Lyman-α transition from 0 to 400 eV by electron impact on CH_4. The data points occur in steps of 0.4 eV and were obtained in the static gas mode. Comparison with other experimental work is made in inset below which show data in 0.1 eV steps.

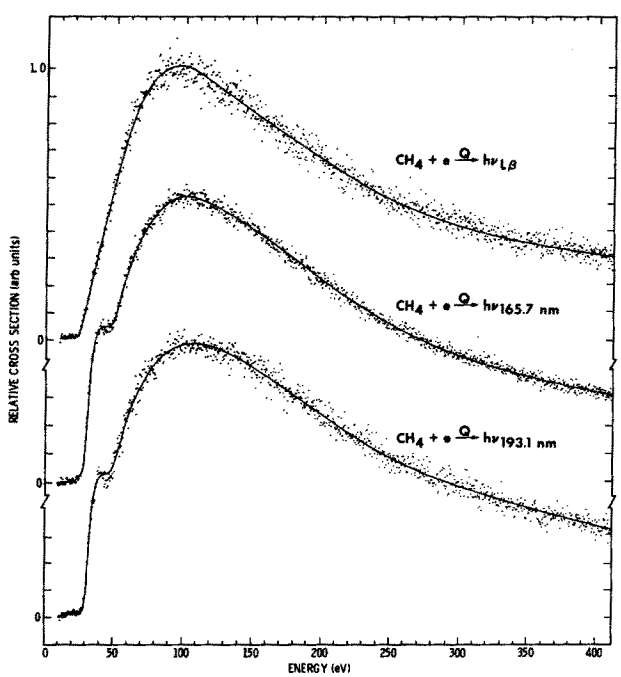

FIG. 8. Relative emission cross section of Lyman-β, and CI (165.7 and 193.1 nm) from 0–400 eV by electron impact of CH_4.

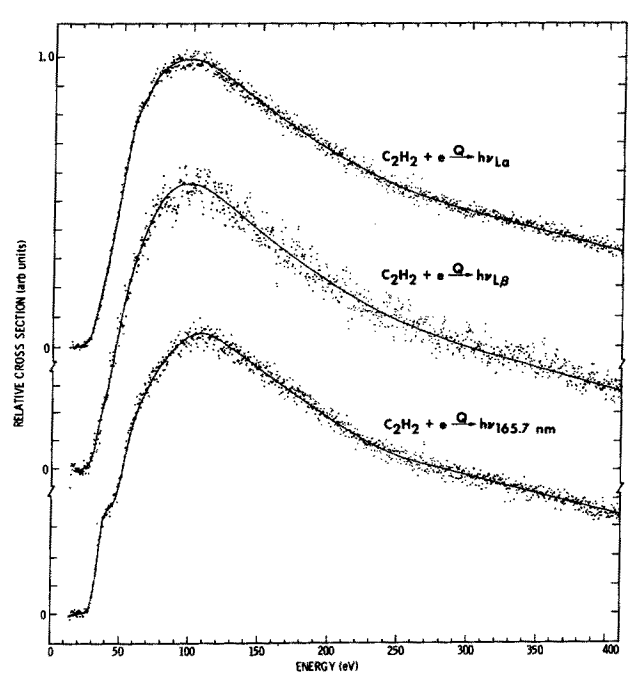

FIG. 9. Relative emission cross section of Lyman-α, and Lyman-β, and C I (165.7 nm) from 0–400 eV by electron impact of C_2H_2.

TABLE I. Electron impact excitation cross sections for CH_4 and C_2H_2.

	CH_4				C_2H_2		
Energy	Q(Ly-α) 10^{-18} cm^2	Q(Ly-β) 10^{-19} cm^2	Q(165.7 nm) 10^{-19} cm^2	Q(193.1 nm) 10^{-19} cm^2	Q(Ly-α) 10^{18} cm^2	Q(Ly-β) 10^{-19}cm^2	Q(165.7 nm) 10^{-19} cm^2
20.0	0.01	0.00	0.00	0.01	0.00	0.00	0.04
22.5	0.04	0.02	0.01	0.01	0.06	0.00	0.07
25.0	0.18	0.29	0.06	0.01	0.15	0.00	0.16
27.5	0.40	0.74	0.15	0.05	0.34	0.28	0.65
30.0	0.70	1.17	0.65	0.30	0.53	0.61	1.52
32.5	1.10	1.80	1.61	0.70	0.78	0.91	2.71
35.0	1.50	2.24	2.17	0.92	1.06	1.70	3.26
37.5	1.91	2.67	2.48	1.12	1.33	1.94	3.70
40.0	2.41	2.99	2.62	1.19	1.67	2.75	3.83
42.5	2.88	3.65	2.60	1.12	1.97	3.11	4.11
45.0	3.24	4.01	2.61	1.11	2.34	3.66	4.33
47.5	3.63	4.71	2.63	1.15	2.65	4.03	4.86
50.0	4.01	5.16	2.76	1.29	2.92	4.48	5.38
52.5	4.34	5.54	2.96	1.40	3.24	4.71	6.11
55.0	4.66	6.07	3.13	1.43	3.50	5.35	6.73
57.5	4.96	6.42	3.40	1.62	3.69	5.98	7.19
60.0	5.18	6.85	3.65	1.69	3.83	5.93	7.61
62.5	5.36	7.24	3.81	1.75	3.90	6.42	7.90
65.0	5.53	7.28	3.92	1.85	4.04	6.76	8.18
67.5	5.68	7.67	4.02	1.89	4.17	6.59	8.32
70.0	5.88	7.97	4.23	1.98	4.27	7.32	8.73
72.5	5.93	8.16	4.32	1.99	4.30	7.38	8.86
75.0	6.02	8.09	4.40	2.06	4.42	7.53	8.97
77.5	6.10	8.33	4.45	2.03	4.39	7.93	9.13
80.0	6.14	8.55	4.59	2.10	4.43	7.71	9.25
82.5	6.27	8.39	4.52	2.15	4.53	7.74	9.49
85.0	6.29	8.50	4.68	2.15	4.57	7.53	9.72
87.5	6.35	8.73	4.80	2.19	4.56	7.43	9.85
90.0	6.40	8.56	4.78	2.21	4.56	8.25	9.93
92.5	6.39	8.74	4.81	2.22	4.57	8.29	9.90
95.0	6.37	8.65	4.85	2.26	4.56	8.15	10.10
97.5	6.36	8.43	4.82	2.25	4.59	7.90	10.16
100.0	6.34	8.55	4.89	2.25	4.56	8.12	10.22
120.0	6.08	8.07	4.71	2.20	4.29	7.74	9.96
140.0	5.76	7.59	4.44	2.13	3.96	7.09	9.32
160.0	5.28	6.80	4.09	1.98	3.67	6.34	8.59
180.0	4.86	6.15	3.73	1.81	3.39	5.87	7.95
200.0	4.44	5.62	3.39	1.65	3.10	5.20	7.15
220.0	4.08	5.04	3.07	1.49	2.85	4.64	6.45
240.0	3.74	4.52	2.77	1.36	2.61	4.31	5.96
260.0	3.41	4.18	2.54	1.24	2.46	4.02	5.57
280.0	3.17	3.87	2.31	1.14	2.32	3.59	5.25
300.0	2.98	3.62	2.14	1.07	2.19	3.42	4.98
320.0	2.76	3.28	2.01	0.98	2.10	3.12	4.76
340.0	2.60	3.03	1.84	0.89	1.98	3.00	4.48
360.0	2.44	2.91	1.70	0.82	1.88	2.78	4.21
380.0	2.29	2.75	1.60	0.79	1.74	2.40	3.92
400.0	2.18	3.93	1.51	0.73	1.63	2.14	3.63

8. The analysis of the excitation function for the threshold region and the high-energy region is described below.

V. THRESHOLD STUDIES

At the resolution of 0.5 eV/channel in Fig. 7 (upper panel) and Figs. 8 and 9 the H Lyman-α and H Lyman-β excitation functions from CH_4 and C_2H_2 appear to have a single threshold, while the C I excitation functions (Figs. 8 and 9) show two appearance potentials. The single and double thresholds have been observed by previous experimenters.[19,26–30]

However, theoretical considerations suggest that there should be a whole series of thresholds, rather than just one or two. Sroka[19] showed that excited H atoms can be produced from methane by at least six processes with minimum electron impact energies calculated to be between 14.7 to 27.3 eV for H Lyman-α, and between 17.6 to 30.2 eV for Lyman-β. Morgan and Mentall[28] computed essentially the same six Lyman-α thresholds for methane. In addition Ref. 28 found three theoretical thresholds each for the C I lines at 156.1 and 165.7 nm, and these varied from 20.60 to 38.73 eV, and 20.10 to 38.23 eV, respectively. It appears that the failure to

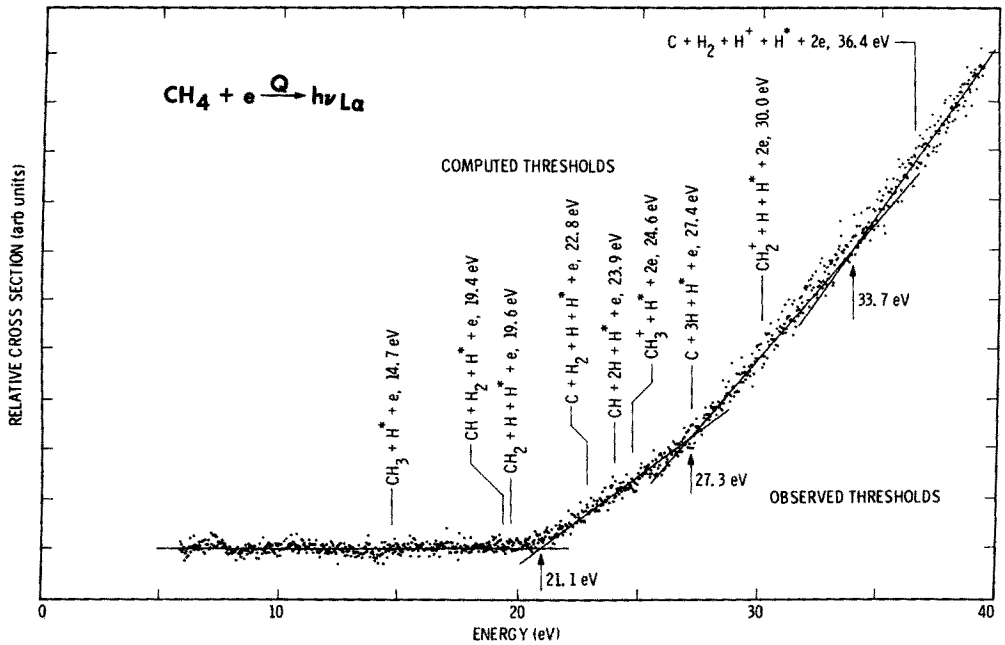

FIG. 10. Relative emission cross section of Lyman-α from 0 to 40 eV by electron impact of CH_4. The data points occur every 0.04 eV. The energies below the curve indicate the experimental appearance potentials. The processes above the curve indicate some of the possible dissociation limits. The processes are also listed in Table II.

observe more than one or two thresholds by these authors may be caused by low instrumental resolution or detector sensitivity or both. Our instrumental electron energy resolution is 0.5 eV FWHM, and our signal statistics 1σ variation is less than 5%. Indeed, when our instrument was programmed to make repetitive scans from only 10 to 110 eV, rather than 10 to 410 eV, the higher-resolution data (0.1 eV per data point) show what appears to be a series of thresholds for Lyman-α, rather than just one. See lower panel of Fig. 7. These thresholds become quite obvious for the higher resolution of Lyman-α data on a scale of 0–40 eV in Fig. 10.

A. H Lyman-α and H Lyman-β

Figure 10 shows that the methane excitation function has definite "breaks" in slope or inflection points in the threshold region. This is the region where the cross sections for each process vary approximately linearly with energy. The threshold energy for each process can be determined by fitting straight lines to data intervals that vary linearly and finding their intercept. This procedure was used by Becker *et al.*[32] to determine a series of AP's for electron impact dissociative excitation of SO_2, and by Donahue *et al.*[9] for interpreting the optical excitation functions of excited fragments from CH_4. Three AP's were so found for Lyman-α from CH_4, indicated by arrows at 21.1, 27.3, and 33.7 eV in Fig. 10.

Theoretical DL for Lyman-α production were computed in Table II for 11 processes that leave the undetected fragment(s) in the ground state(s) and all fragments at rest at infinity. We have compared the DL to the observed AP in order to determine the range of values of the kinetic energy of the excited H ($2p$) fragment. The kinetic energy released in the dissociation process imparts highly nonthermal velocities to the H fragments. Most of the kinetic energy goes to the H fragment.

For reaction (1) in Table II (and similarly for other

TABLE II. Dissociation limits (DL), appearance potentials (AP), and reaction energies of products (E) for CH_4 at Ly-α.

Process for Ly-α $CH_4 + e \rightarrow$	Dissociation limit for 300 K DL (eV)	E, reaction energy of products at AP, E = AP-DL (eV)		
		AP (eV)[a] = 21.1	27.3	33.7
(1) $CH_3 + H^* + e$	14.7	6.4	12.6	19.0
(2) $CH + H_2 + H^* + e$	19.4	1.7	7.9	14.3
(3) $CH_2 + H + H^* + e$	19.6	1.5	7.7	14.1
(4) $C + H_2 + H + H^* + e$	22.8		4.5	10.9
(5) $CH + 2H + H^* + e$	23.9		3.4	9.8
(6) $CH_3^+ + H^* + 2e$	24.6		2.7	9.1
(7) $C + 3H + H^* + e$	27.4			6.3
(8) $CH_2^+ + H + H^* + 2e$	30.0			3.7
(9) $C + H_2 + H^+ + H^* + 2e$	36.4			
(10) $C + 2H + H^+ + H^* + 2e$	41.0			
(11) $C^+ + 3H + H^* + e$	98.0			

[a] Appearance potentials from previous work: (Morgan and Mentall, Ref. 28) 21.9 eV; (Sroka, Ref. 19) 20.7 eV; (McGowan *et al.*, Ref. 27) 19 eV; (Orient and Srivastava, Ref. 30) 25 eV; (Mohlmann *et al.*, Ref. 29) 20.0 eV.

TABLE III. Dissociation limits (DL), appearance potentials (AP), and reaction energies of products (E) for C_2H_2 at Ly-α.

Process for Ly-α $C_2H_2 + e \rightarrow$	Dissociation limit for 300 K DL(eV)	E, reaction energy of products at AP, E = AP-DL (eV)			
		AP (eV) = 16.3	21.0	27.9	39.7
(1) $C_2H + H^* + e$	15.1	1.2	5.9	12.8	24.6
(2) $C_2 + H + H^* + e$	21.1			6.8	18.6
(3) $C + CH + H^* + e$	23.7			4.2	16.0
(4) $C + C + H + H^* + e$	27.2			9.7	12.5
(5) $C_2H^+ + H^* + 2e$	32.3				7.4
(6) $C_2^+ + H + H^* + 2e$	33.0				6.7
(7) $C + C + H^+ + H^* + 2e$	40.8				
(8) $C^+ + C + H + H^* + 2e$	97.8				

CH_4 reactions in Tables II and IV and C_2H_2 reactions in Tables III and IV, see Schiavone *et al.*[7]) the kinetic energy, T, of the H fragment is given by

$$T = \tfrac{15}{16}\beta E, \tag{4}$$

where E is excess reaction energy released and β is fraction of excess reaction energy going into translational energy. Schiavone *et al.*[7] have measured values of $0.5 < \beta < 1$ for CH_4. It appears that excited H fragments from CH_4 at least in the high Rydberg case[7] occurs with the majority of the energy as translational energy.

The first AP at 21.1 eV can give rise to products with energy 6.4, 1.7, and 1.5 eV for reactions 1, 2, 3, respectively. The doppler width would be anticipated to be 70–140 mÅ for $\beta = 1$. Thus a measurement of the line shape in the threshold energy region remains an important investigation.

Direct comparisons of the results here with another optical emission experiment on CH_4 [9] can be made by comparing our results on Lyman-α with the Balmer-β (486.1 nm) values of Ref. 9. Donahue *et al.*[9] found distinct AP's at 22.0, 27.4, and 36.5 eV. The AP's measured here for Lyman-α from CH_4 occur at 21.1, 27.3, and 33.7 eV. We note a similar series of thresholds for Lyman-α formation from C_2H_2 of 16.3, 21.0, 27.9, and 39.7 eV AP in Table III. To our knowledge, this is the first time the first AP of Lyman-α from these hydrocarbons below 20 eV has been measured.

For CH_4 the first AP at 21.1 eV for Lyman-α agrees well with the first AP of Balmer-β at 22.0 eV. These AP's agree, in turn, with analyses of high Rydberg production $15 < n < 80$ found in time of flight experiments by Finn *et al.*[8] and Schiavone *et al.*[7] AP's for production of high Rydberg atoms occurred at 22.0, 25.5, 36.7, and 66 eV from Ref. 8 and 24.5, 26.4, 34.8, and 74 eV from Ref. 7. Schiavone *et al.*[7] have measured the kinetic energy distribution to be $4 < T < 8$ eV for the 24.5 eV AP with $\beta = 0.81$. Donahue *et al.*[9] have inferred, based on the core–ion model of Rydberg potential curves, that excitation of high Rydberg atoms and the $n = 4$ Balmer-β level are similar. Thus the AP in the optical emission experiments[9] at 22 eV correlates with the first AP of high Rydberg production.[7] The high Rydberg production with kinetic energy of 4 to 8 eV correlates to the dissociation limit of a ground methyl radical with some vibrational energy and a hydrogen atom. Thus Donahue *et al.*[9] infer the selection of CH_3 and H as the main production process at the first Balmer-β threshold. Similarly, we suggest that process (1) in Table II is the main dissociative route for the first AP.

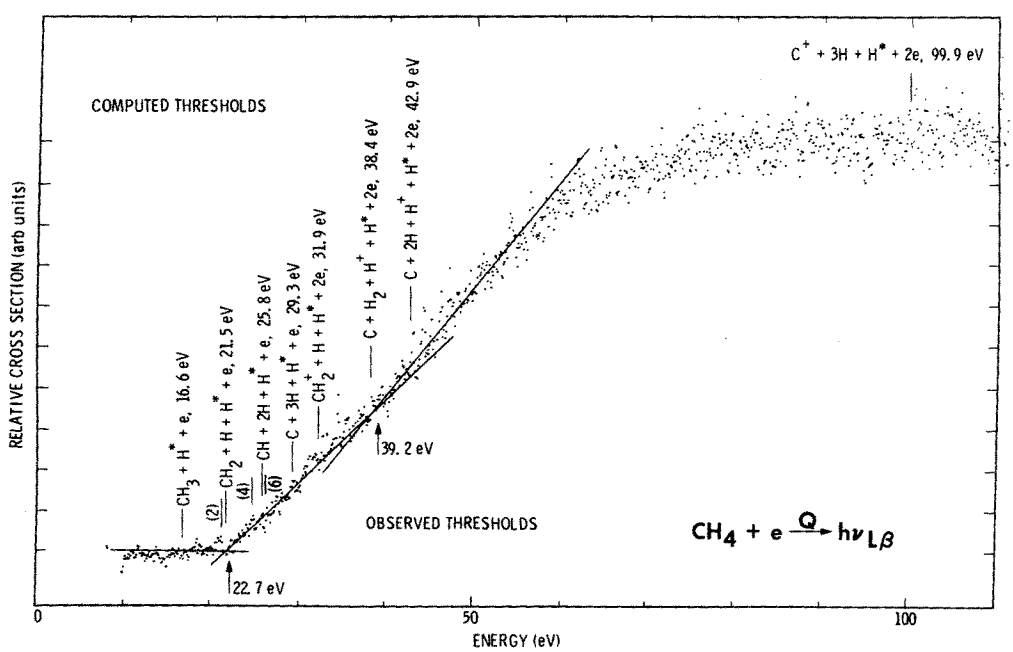

FIG. 11. Relative emission cross section of Lyman-β from 0 to 110 eV by electron impact of CH_4. The data points occur every 0.1 eV. The energies below the curve indicate the experimental appearance potentials. The processes above the curve indicate some of the possible dissociation limits. The processes are also listed in Table IV.

The kinetic energy of the H($2p$) fragment would be ~ 5 eV for $\beta = 0.8$. This number is in excellent agreement with the predicted kinetic energy of a fragment H($2p$) atom following dissociation based on analysis, given earlier, for the spectra in Figs. 1 and 3.

Sroka[19] and Morgan and Mentall[28] found that there is a difference of several eV between the measured AP and the computed DL for what they believed to be the dominant dissociative excitation process. For example, Morgan and Mentall considered the process

$$CH_4 + e \rightarrow CH + H_2 + H^* + e \quad (5)$$

to be the most important and attributed it to a 21.9 eV observed threshold. The difference between this experimental value and their DL is 2.6 eV, which is imparted as vibrational and kinetic energy to the fragments.[28] Sroka measured an AP of 20.7 and 21.2 eV for Lyman-α and Lyman-β, respectively, and considered the above process as well as the processes

$$CH_4 + e \rightarrow CH_3 + H^* + e \quad (6)$$

and

$$CH_4 + e \rightarrow CH_2 + H + H^* + e, \quad (7)$$

to be energetically possible also. Table II shows that four groups of experimenters determined a nearly equal AP at 20–22 eV. Our analysis and that of Donahue *et al.*[9] show this AP most likely marks the onset of process (1) in Table II.

For the remaining AP's for Lyman-α it is not possible to attribute them to a single excitation process of CH_4. We list in Tables II and III the exothermic reaction energy for all possible processes involving Lyman-α from CH_4 and C_2H_2.

As discussed at the end of the last section the data for the excitation function of methane at Lyman-β has much greater scatter, despite longer integration times and three-point data smoothing. Analysis of the data in Fig. 11 produced only one additional threshold due to the reduced signal-to-noise ratio. Therefore, detection of additional thresholds requires measurements with higher signal-to-noise ratio.

Analysis of the data in Fig. 11 produced the two AP's for Lyman-β at 22.7 and 39.2 eV for CH_4. Similarly, analysis of the data in Fig. 15 showed two thresholds at 21.0 and 30.0 eV for C_2H_2. Table IV lists the AP's for Lyman-β from CH_4 and C_2H_2, respectively, and indicates limits for the same processes as for Lyman-α. The AP's for Lyman-β seem to correlate with corresponding AP's for Lyman-α.

B. The C I lines

The high resolution electron impact excitation functions for the 165.7 and 193.1 nm multiplets of C I from CH_4 are shown in Figs. 12 and 13 and for the 165.7 nm multiplet of C I from C_2H_2 in Fig. 16. We list in Table V the observed AP's and the candidate processes that involve a ground state product for the undetected fragment(s).

We note in each case, three distinct AP's for the C I lines. The first two AP's for both CH_4 and C_2H_2 correspond

TABLE IV. Observed appearance potentials for CH_4 and C_2H_2 at Ly-β.

Process for Ly-β: $CH_4 + e \rightarrow$	Dissociation limit for 300 K DL (eV)	Appearance potential[a] AP (eV)	
		22.7	39.2
(1) $CH_3 + H^* + e$	16.6		
(2) $CH + H_2 + H^* + e$	21.3		
(3) $CH_2 + H + H^* + e$	21.5		
(4) $C + H_2 + H + H^* + e$	24.8		
(5) $CH + 2H + H^* + e$	25.8		
(6) $CH_3^+ + H^* + 2e$	26.5		
(7) $C + 3H + H^* + e$	29.3		
(8) $CH_2^+ + H^* + H + 2e$	31.9		
(9) $C + H_2 + H^+ + H^* + 2e$	38.4		
(10) $C + 2H + H^+ + H^* + 2e$	42.9		
(11) $C^+ + 3H + H^* + 2e$	99.9		

Process for Ly-β: $C_2H_2 + e \rightarrow$	Dissociation limit for 300 K DL (eV)	Appearance potential AP (eV)	
		21.0	30.0
(1) $C_2H + H^* + e$	17.0		
(2) $C_2 + H + H^* + e$	23.0		
(3) $C + CH + H^* + e$	25.6		
(4) $C + C + H + H^* + e$	29.1		
(5) $C_2H^+ + H^* + 2e$	34.2		
(6) $C_2^+ + H + H^* + 2e$	34.9		
(7) $C + C + H^+ + H^* + 2e$	42.7		
(8) $C^+ + C + H + H^* + 2e$	99.7		

[a] Previous work: 21.2 eV (Sroka, Ref. 19).

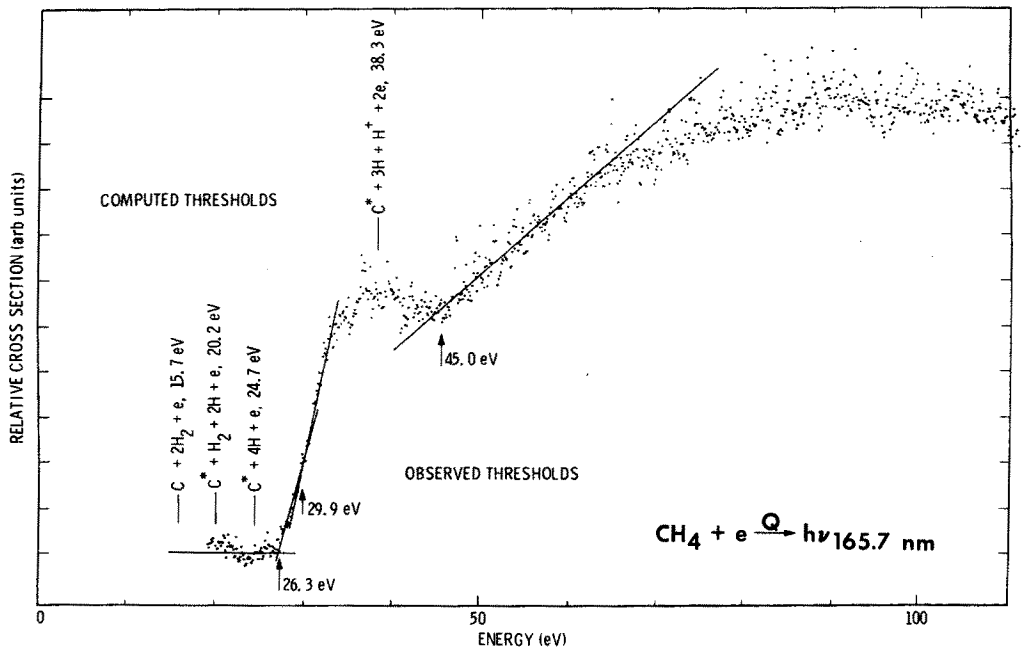

FIG. 12. Relative emission cross section of C I (165.7 nm) from 0 to 110 eV by electron impact of CH_4. The data points occur every 0.1 eV. The energies below the curve indicate the experimental appearance potentials. The processes above the curve indicate some of the possible dissociation limits. The processes are also listed in Table V.

to dissociative excitation involving only neutrals. Three reactions (1)–(3) are noted for CH_4 corresponding to these first two AP's. These cases allow DL's consisting of ground state H atoms or/and H_2 molecules. The only previous work to note three AP's on the C I multiplets from CH_4 was performed by Donahue *et al.*,[9] who studied the C I (193.1 nm) multiplet at about 0.3 eV resolution. They measured AP's of 24.8, 28.0, and 43.0 eV which compare favorably to our AP's of 26.2, 29.6, and 45.1 eV. Previous low energy resolution work by Morgan and Mentall[28] noted two AP's at 25.6 and 43 eV (see Donahue *et al.*[9]). Sroka[19] reported only one AP at 26.2 eV. In addition, Morgan and Mentall[28] reported two AP's for CI (165.7 nm) of 27.3 and 43.4 eV.

It is not possible to decide on the optical emission data alone whether only one or perhaps all energetically allowed processes are involved in the first two thresholds. The onset for the formation of H^+ is clearly seen in the CI excitation functions as a third threshold of Figs. 12, 13, and 16. The released energy E, for this dissociative ionization process is 6.7 eV for 165.7 nm and 7.8 eV for 193.1 nm of CH_4 and 0.8 eV for 165.7 nm of C_2H_2. The equivalent expression to Eq. (4) for the kinetic energy of the C I fragments from CH_4 is

$$T = \tfrac{1}{16}\beta E. \tag{8}$$

Thus in all cases in Table V, even for $\beta = 1$, we expect the kinetic energy of the C fragment to be under 1 eV. The inter-

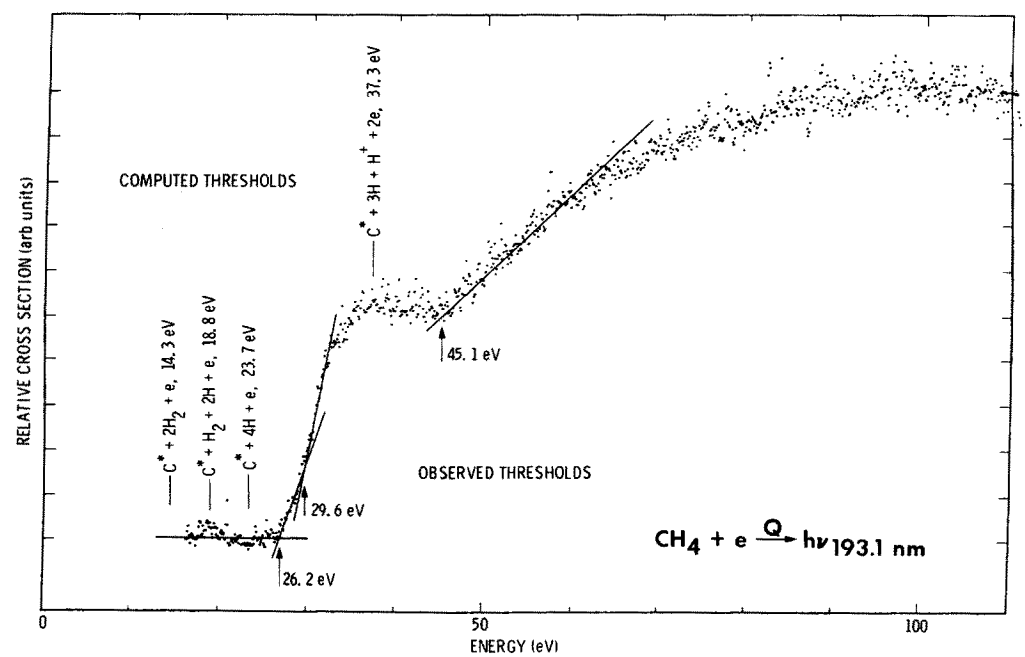

FIG. 13. Relative emission cross section of C I (193.1 nm) from 0 to 110 eV by electron impact of CH_4. The data points occur every 0.1 eV. The energies below the curve indicate the experimental appearance potentials. The processes above the curve indicate some of the possible dissociation limits. The processes are also listed in Table V.

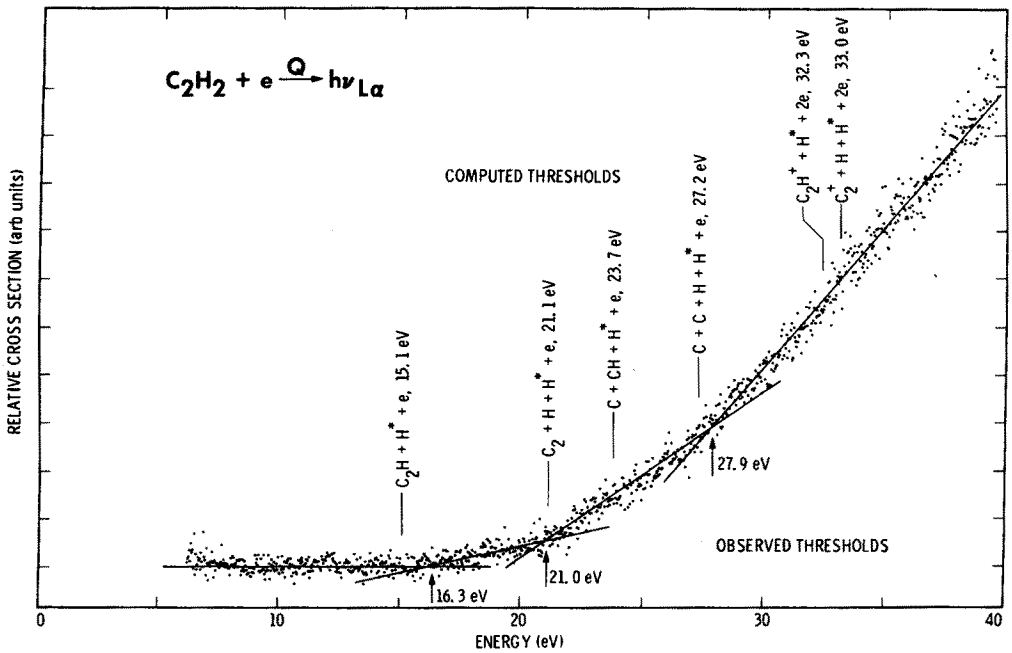

FIG. 14. Relative emission cross section of Lyman-α from 0 to 40 eV by electron impact of C_2H_2. The data points occur every 0.04 eV. The energies below the curve indicate the experimental appearance potentials. The processes above the curve indicate some of the possible dissociation limits. The processes are also listed in Table III.

mediate state is probably a molecular ion with a repulsive potential curve.

Time of flight experiments by Schiavone *et al.*[7] on high Rydberg states of C I from CH_4 confirm this result. They find $0 < T < 1.2$ eV with a peak near 0.3 eV in the kinetic energy distribution.

VI. BETHE–BORN APPROXIMATION

The threshold analysis given in the last section allows us to determine which of the processes are important for the formation of an atomic state. Additional information about the molecular transitions involved can be obtained by analyzing data taken in the high energy region, $\epsilon > 250$ eV. In contrast to the threshold region the slope of the collision strength, $Q\epsilon$, vs $\ln \epsilon$ on a Fano plot determines whether the production of excited fragments by dissociative excitation from a CH_4 intermediate state or/and ionization–dissociation from a CH_4^{**} intermediate state occurs via dipole allowed or forbidden transitions.

Bethe[34] showed that the cross section for dipole transitions is given by

$$Q = \frac{4\pi a_0^2 R}{\epsilon} m_d^2 \ln\left(\frac{4C_n\epsilon}{R}\right), \tag{9}$$

where a_0 is the first Bohr radius, R is the Rydberg energy, ϵ is the energy of the incident electron, m_d^2 is related to the opti-

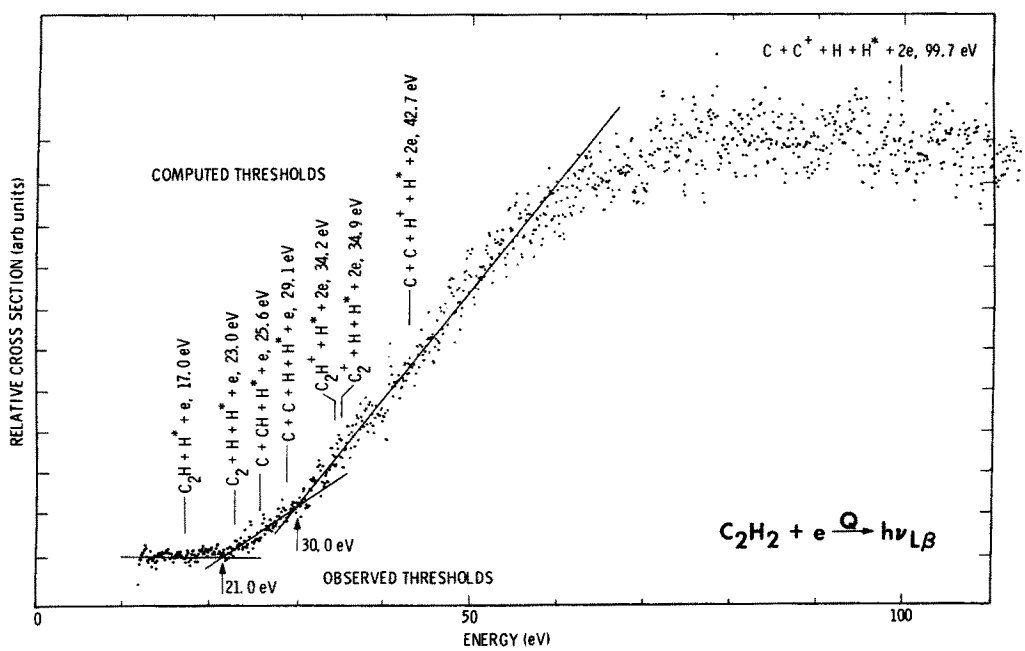

FIG. 15. Relative emission cross section of Lyman-β from 0 to 110 eV by electron impact of C_2H_2. The data points occur every 0.1 eV. The energies below the curve indicate the experimental appearance potentials. The processes above the curve indicate some of the possible dissociation limits. The processes are also listed in Table IV.

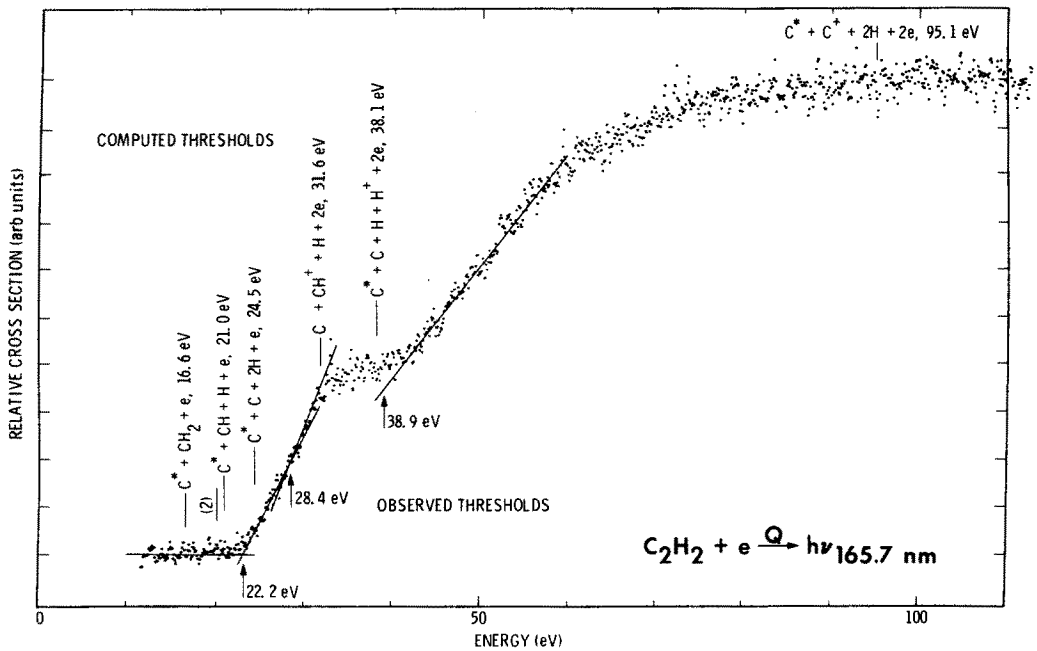

FIG. 16. Relative emission cross section of CI (165.7 nm) from 0 to 110 eV by electron impact. The data points occur every 0.1 eV. The energies below the curve indicate the experimental appearance potentials. The processes above the curve indicate some of the possible dissociation limits. The processes are also listed in Table V.

cal oscillator strength for dissociation to the relevant intermediate state(s) and is defined as the effective dipole moment,[35] and C_n is a constant dependent on the properties of these states. Plotting $(Q\epsilon)/(4\pi a_0^2 R)$ against $\ln \epsilon$ in a Fano plot scatter diagram determines the slope m_a^2 of the straight line of best fit. A positive slope indicates optically allowed transitions, and a negative or zero slope–forbidden transitions.[34,35] Figure 17 is an example of a Fano plot, the data for which is taken from Fig 9. A straight line was fitted to the data points with energy greater than 250 eV by the method of

TABLE V. Dissociation limits (DL), appearance potentials (AP), and reaction energies of products (E) for C I lines from CH_4 and C_2H_2.

Process for C I (165.72 nm): $CH_4 + e \rightarrow$	Dissociation limit for 300 K DL (eV)	E, reaction energy of products at AP, E = AP-DL (eV)		
		AP (eV)[a] = 26.3	29.9	45.0
(1) $C^* + 2H_2$	15.7	10.6	14.2	
(2) $C^* + H_2 + 2H + e$	20.2	6.1	9.7	
(3) $C^* + 4H + e$	24.7	1.6	5.2	
(4) $C^* + 3H + H^+ + 2e$	38.3			6.7
Process for C I (193.09 nm): $CH_4 + e \rightarrow$	Dissociation limit for 300 K DL (eV)	E, reaction energy of products at AP, E = AP-Dl (eV)		
		AP (eV)[a] = 26.2	29.6	45.1
(1) $C^* + 2H_2$	14.3	11.9	15.3	
(2) $C^* + H_2 + 2H + e$	18.8	7.4	10.8	
(3) $C^* + 4H + e$	23.7	2.5	5.9	
(4) $C^* + 3H + H^+ + 2e$	37.3			7.8
Process for C I (165.72 nm): $C_2H_2 + e \rightarrow$	Dissociation limit for 300 K DL (eV)	E, reaction energy of products at AP, E = AP-DL (eV)		
		AP (eV) = 22.2	28.4	38.9
(1) $C^* + CH_2 + e$	16.6	5.6	11.8	
(2) $C^* + C + H_2 + e$	20.0	2.2	8.4	
(3) $C^* + CH + H + e$	21.0	1.2	7.4	
(4) $C^* + C + 2H + e$	24.5		3.9	
(5) $C^* + CH^+ + H + 2e$	31.6			7.3
(6) $C^* + C + H + H^+ + e$	38.1			0.8
(7) $C^* + C^+ + 2H + 2e$	95.1			

[a] Appearance potentials from previous work: 165.72 nm, AP = 26.2 eV (Sroka, Ref. 19) 27.3 and 43.4 eV (Morgan and Mentall, Ref. 28), and 193.09 nm, AP = 24.8, 28.0, and 43.0 eV. (Donahue *et al.*, Ref. 9).

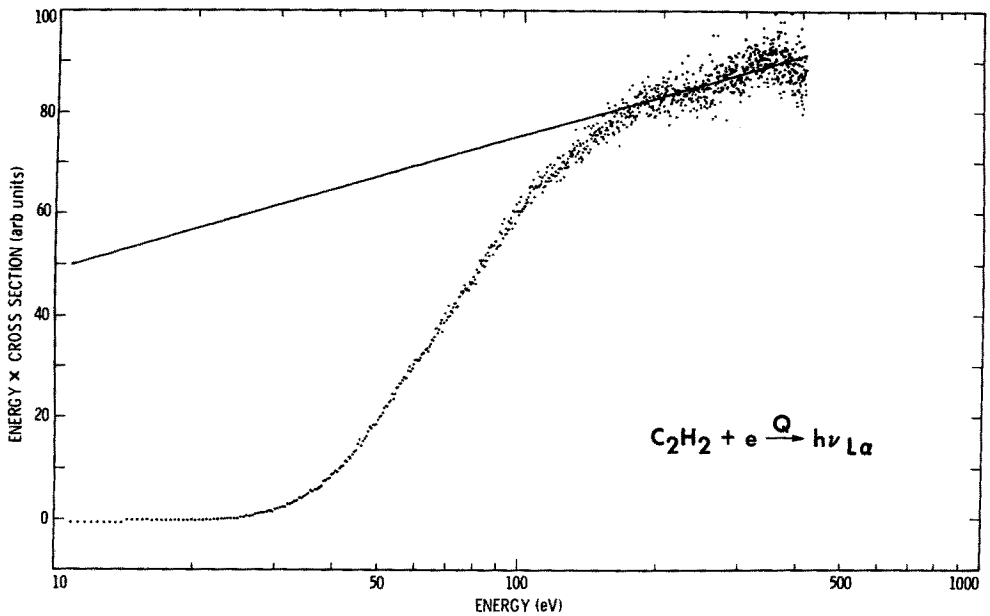

FIG. 17. Fano plot of $Q\epsilon$ = collision strength in arbitrary units vs ln ϵ for Lyman-α from electron excitation of C_2H_2. In absolute units the equation of the straight line is $Q\epsilon = 8.815\times10^{-17}$ [ln $\epsilon + 2.0034$] with Q in cm^2 and ϵ in eV.

least squares. The ordinate is still in arbitrary units so that the m_d^2 values found from the regression analysis have to be standardized by an absolute calibration. The absolute m_d^2 value for the C_2H_2 Lyman-α emissions is 0.0736. The positive slope of the regression line indicates that the dominant high energy transition involved is optically allowed. Fano plots of all the other emissions have negative or zero slopes and are thus classified as forbidden transitions. However our energy range of 250 to 400 eV is limited.

In agreement, Mohlmann *et al.*[29] find the Lyman-α transition, dissociatively excited from CH_4, to be forbidden. Time of flight spectra on CH_4, Schiavone *et al.*,[7] indicate that for high quantum number Rydberg H atoms the dissociative processes which have AP's in the 30–70 eV region have the largest cross section at high energies. This may be true for the Lyman-α and Lyman-β cross sections measured here indicating the dominance of ionization–dissociation at high energy.

Donahue *et al.*[9] determine the dissociation process of CH_4 leading to the CI (183.1 nm) transition to be optically forbidden.

ACKNOWLEDGMENTS

This work was jointly carried out by Jet Propulsion Laboratory, California Institute of Technology, Pasadena, CA 91109; University of Southern California, Los Angeles, CA 90089; and the University of Arizona, Tucson, AZ 85717; and supported by the National Science Foundation, the Air Force Office of Scientific Research (AFOSR), and the NASA Planetary Sciences and Astronomy/Relativity Programs.

[1]R. Hanel, B. Conrath, F. M. Flaser, V. Kunde, W. Maguire, J. Pearl, J. Pirraglia, R. Samuelson, D. Cruikshank, D. Gautier, P. Gierasch, L. Horn, and C. Ponnamperuma, Science **215**, 544 (1982).

[2]A. L. Broadfoot, F. Herbert, J. B. Holberg, D. M. Hunten, S. Kumar, B. R. Sandel, D. E. Shemansky, G. R. Smith, R. V. Yelle, D. F. Strobel, H. W. Moos, T. M. Donahue, S. K. Atreya, J. L. Bertaux, J. E. Blamont, J. C. McConnell, A. J. Dessler, S. Linick, and R. Springer, Science **233**, 74 (1986).

[3]S. K. Atreya, *Uranus and Neptune*, edited by J. T. Bergstralh, NASA Conf. Publ. 2330, 1984, pp. 55–88.

[4]J. Clarke, S. Durrance, S. Atreya, A. Barnes, J. Belcher, M. Festou, C. Imhoff, J. Mihalov, W. Moos, J. Murthy, A. Pradhan, and T. Skinner, J. Geophys. Res. **91**, 8771 (1986).

[5]J. M. Ajello, D. Shemansky, T. L. Kwok, and Y. L. Yung, Phys. Rev. A **29**, 636 (1984).

[6]D. E. Shemansky, J. M. Ajello, and D. T. Hall, Astrophys. J. **296**, 765 (1985).

[7]J. A. Schiavone, D. E. Donahue, and R. S. Freund, J. Chem. Phys. **67**, 759 (1977).

[8]T. G. Finn, B. L. Carnahan, W. C. Wells, and E. C. Zipf, J. Chem. Phys. **63**, 1596 (1975).

[9]D. E. Donahue, J. A. Schiavone, and R. S. Freund, J. Chem. Phys. **67**, 769 (1977).

[10]J. M. Ajello and S. K. Srivastava, J. Chem. Phys. **75**, 4454 (1981).

[11]J. M. Ajello, S. K. Srivastava, and Y. L. Yung, Phys. Rev. A **25**, 2485 (1982).

[12]J. M. Ajello and D. E. Shemansky, J. Geophys. Res. **90**, 9845 (1985).

[13]R. J. Van Brunt and R. N. Zare, J. Chem. Phys. **48**, 4304 (1968).

[14]S. K. Srivastava, A. Chutjian and S. Trajmar, J. Chem. Phys. **63**, 2659 (1975); S. Trajmar and D. Register, *Electron Molecule Collisions*, edited by K. Takayanagi and I. Shimamura (Plenum, New York, 1984), Chap. 6.

[15]Based on average of 7.3×10^{-18} cm^2 for four measurements at 100 eV: Ref. 6 value of 8.18×10^{-18} cm^2, W. McConkey (private communication) value of 7.2×10^{-18} cm^2, R. G. Ligtenberg, A. McPherson, N. Rouze, W. Westerveld, and J. S. Risley, Abstracts of Contributed Papers of the XIVth International Conference on the Physics of Electronic and Atomic Collisions, p. 276, Palo Alto, CA (1985) value of 6.57×10^{-18} cm^2 and B. Van Zyl, M. Gealy, and H. Neumann, Phys. Rev. A **31**, 2922 (1985) value of 7.22×10^{-18} cm^2. The average value at 100 eV determines the 200 eV cross section from published Lyman-α results of Mumma and Zipf, J. Chem. Phys. **53**, 7661 (1971).

[16]See AIP document no. PAPS JCPSA-86-2750-10 for 10 pages of tables. Order by PAPS number and journal reference from American Institute of Physics, Physics Auxiliary Publication Service, 335 East 45th Street, New York, NY 10017. The price is $1.50 for each microfiche (98 pages) or $5.00 for photocopies of up to 30 pages, and $0.15 for each additional page over 30 pages. Airmail additional. Make checks payable to the American Institute of Physics. The spectral identifications used in these tables are based on the work of R. L. Kelly and L. J. Palumbo, Atomic and Ionic Emission Lines Below 2000A: Hydrogen through Krypton, Rep. 7599, Nav. Res. Lab., Washington, D.C., pp. 46–52 (1973).

[17]J. T. Tate and D. T. Smith, Rev. Mod. Phys. **39**, 270 (1932); H. Chatham,

D. Hils, R. Robertson, and A. Gallagher, J. Chem. Phys. **81**, 1770 (1984); A. Gaudin and R. Hagemann, J. Chim. Phys. **64**, 1209 (1967).
[18]O. J. Orient and S. K. Srivastava, J. Phys. B (in press); D. Rapp, P. Englander-Golden, and D. D. Briglia, J. Chem. Phys. **42**, 4081 (1965).
[19]W. Sroka, Z. Naturforsch. **249**, 1724 (1969).
[20]H. F. Winters, J. Chem. Phys. **63**, 3462 (1975).
[21]J. F. M. Aarts and F. J. de Heer, Physica **56**, 294 (1971).
[22]D. E. Shemansky and J. M. Ajello, J. Geophys. Res. **88**, 459 (1983).
[23]W. L. Wiese, M. W. Smith, and B. M. Glennon, *Atomic Transition Probabilities. Vol. 1. Hydrogen Through Neon,* Natl. Stand. Ref. Data Ser. 1 (U. S. GPO, Washington, D.C., 1966).
[24]E. C. Zipf, *Electron–Molecule Interactions and Applications. Vol. 1,* edited by L. G. Christophorou (Academic, New York, 1984), Chap. 4.
[25]R. S. Freund, J. A. Schiavone, and D. F. Brader, J. Chem. Phys. **64**, 1122 (1976).
[26]D. A. Vroom and F. J. de Heer, J. Chem. Phys. **50**, 573 (1969).
[27]J. W. McGowan, J. F. Williams, and D. A. Vroom, Chem. Phys. Lett. **3**, 614 (1969).
[28]H. D. Morgan and J. E. Mentall, J. Chem. Phys. **60**, 4734 (1974).
[29]G. R. Mohlmann, K. H. Shima, and F. J. de Heer, Chem. Phys. **28**, 331 (1978).
[30]O. J. Orient and S. K. Srivastava, Chem. Phys. **54**, 183 (1981).
[31]R. W. McLaughlin and E. C. Zipf, Chem. Phys. Lett. **55**, 62 (1978).
[32]K. Becker, W. Van Wijngarden, and J. W. McConkey, Planet. Space Sci. **31**, 197 (1983).
[33]H. M. Rosenstock, K. Draxl, B. W. Steiner, and J. T. Herron, *Energetics of Gaseous Ions.*, J. Phys. Chem. Ref. Data, Vol. 6 (National Bureau of Standards, Washington, D. C., 1977).
[34]H. A. Bethe, Ann. Phys. **5**, 325 (1930).
[35]F. J. de Heer, Int. J. Radiat. Phys. Chem. **7**, 137 (1975).